Abrinaei *Journal of the European Optical Society-Rapid Publications* (2017) 13:15
DOI 10.1186/s41476-017-0042-z

Journal of the European Optical Society-Rapid Publications

RESEARCH Open Access

Nonlinear optical response of Mg/MgO structures prepared by laser ablation method

Fahimeh Abrinaei

Abstract

Background: Investigation of new materials plays an important role in advancing the field of optoelectronics.

Methods: In this work, Mg/MgO microstructures were prepared by Nd-YAG laser (λ= 1064 nm) ablation of magnesium target in acetone. For the first time, the nonlinear optical properties of square Mg/MgO microstructures were investigated by using the Z-scan technique with nanosecond Nd-YAG laser at 532 nm.

Results: The XRD analysis approved the formation of Mg/MgO microstructures. The energy band gap of Mg/MgO microstructures was calculated to equal 2.3 eV from UV-Vis spectrum. The ablated materials were ejected into acetone as structures with an average size of 1-1.5 μm. The nonlinear absorption coefficient, β, and nonlinear refractive index, n_2, for Mg/MgO microstructures at the laser intensity of 1.1×10^8 W/cm2 were measured to be 1.15×10^{-8} cm/W and 8.2×10^{-13} cm^2/W, respectively. In order to investigate size particles and liquid medium effects, the nonlinear optical parameters, β and n_2 of Mg/MgO nanostructures synthesized by laser ablation of magnesium target in isopropanol also were calculated and it was found these parameters are an order of magnitude larger than the values for the β and n_2 of Mg/MgO microstructures synthesized in acetone. The third-order nonlinear optical susceptibility, $\chi^{(3)}$, of Mg/MgO microstructures and nanostructures were measured in order of 10^{-6} and 10^{-5} esu, respectively.

Conclusions: The results show that Mg/MgO structures synthesized in acetone and isopropanol have negative nonlinearity as well as good nonlinear absorption at 532 nm and these magnesium-based structures have the potential applications in the nonlinear optical devices.

Keywords: Laser materials processing, Mg/MgO microstructures, Mg/MgO nanostructures, Nonlinear optics, Z-scan technique

Background

Materials with the large nonlinear optical (NLO) response, good capabilities of processing, environmental constancy and ultrafast signal switching are necessary for potential applications in optical signal processing, optical limiting (OL), and optical devices. Designing of new materials with large nonlinearities is a promising line of the current opto-electronics. So, composite particles that are attractive to build various photonic devices provide many unique opportunities to achieve a large optical nonlinearity [1].

In recent years, many researchers have noted to magnesium microstructures and nanostructures due to their novel properties to distinguish them from bulk materials and diverse applications in fields of propellant, battery, composite fillers, etc. Magnesium has several very promising properties for applications in plasmonics and specially in switchable plasmonic metamaterials [2]. As reported by Sterl et al., magnesium nanoparticles exhibit a pronounced plasmonic response at throughout the whole visible wavelength range. Therefore, it can be an ideal alternative to established materials for UV plasmonics such as aluminum [3]. Magnesium is an excellent candidate for weight critical structural applications for its impressive low mass density. A good high-temperature crawl, a high damping capacity,

Correspondence: f_abrinaey@yahoo.com
Department of physics, East Tehran Branch, Islamic Azad University, Tehran, Iran

and good dimensional stability are the properties that make magnesium perfect for industrial applications [4–9]. Magnesium is a candidate for the fuel cell technologies. It is reversible, abundant and low-cost element possesses the large capacity for hydrogen storage (7.6 wt.%) [10].

Magnesium oxide (MgO) nanostructures and microstructures have attracted more and more regard in recent years. MgO is an important inorganic material possesses a wide band gap energy ($E_g \sim 7.8$ eV) [11]. MgO is a useful oxide material for industrial applications. MgO has been employed such as an additive in heavy fuel oils, toxic waste remediation, catalyst supports, refractory materials and adsorbents, catalysis, reflecting and anti-reflecting coatings, superconducting and ferroelectric thin films as the substrate, etc [12, 13]. For medical uses, MgO is used for the sedation of heartburn, sore stomach, and for bone instauration [14, 15]. Recently, researchers have discovered that MgO nanoparticles are appropriate for application in tumor treatment [16]. MgO nanoparticles are suitable for application as antibacterial agent [17].

Kurth et al. reported the initial oxidation of magnesium at oxygen partial pressures and showed that the initially formed oxide has a higher Mg/O ratio (>1.3) than bulk MgO. Also, they indicated that the band gap values of the oxide layers are considerably smaller than the value expected for bulk MgO (2.5 eV vs. 7.8 eV) [18]. Canney et al. studied electronic band structure of thin magnesium and magnesium oxide films, experimentally and theoretically. They showed that the investigated band structures of Mg and MgO have the characteristic of a metallic and ionic solid, respectively [19]. Phuoc et al. synthesized Mg/MgO nanocrystallites by laser ablation of magnesium in acetone and isopropanol with a Q-switched Nd–Yag laser operating at 1064 nm and investigated structural properties of the formed Mg/MgO nanostructures [20]. Abrinaei et al. reported on the study of structural properties of Mg/MgO nanoparticles synthesized by Ng-YAG (λ = 1064 nm) laser as well as CVL (Cooper Vapor Laser) in isopropanol [21]. In the recent months, Gutierrez et al. reported an investigation of the effect of an oxide shell on the ultraviolet plasmonic behavior of Ga, Mg, and Al nanostructures. They studied the plasmonic response of Mg/MgO nanostructures and effect of oxidation on the UV-plasmonic response of Mg/MgO spherical or hemisphere-on-substrate nanostructures [22].

This work analyzes the Mg/MgO microstructures obtained by Nd-YAG (λ = 1064 nm) laser ablation of solid magnesium target in acetone media, through the study of their X-ray diffraction powder pattern, SEM image, Fourier transform infrared spectroscopy (FTIR) spectrum and UV-VIS spectrum. The nonlinear absorption and refraction of these microstructures are investigated by using the Z-scan technique with Nd-YAG laser at 532 nm. Furthermore, the current research discusses the OL properties of Mg/MgO colloids. To compare the case, linear and NLO properties of spherical and platelet-like Mg/MgO nanostructures have been calculated in this work, as well. The synthesis of these nanostructures by Nd-YAG (λ = 1064 nm) laser ablation of magnesium target in isopropanol media and investigation of their structural properties have been already reported in the researcher's previous work [21]. To the best of the author's knowledge, this is the first investigation of NLO properties of Mg/MgO structures induced by the Z-scan method.

Methods

Material synthesis

Mg/MgO microstructures were prepared by laser ablation of Mg metal plate (99.99%) in acetone. As shown in Fig. 1, the target was put at the bottom of a glass vessel filled with 5 ml acetone. The laser beam was focused on the surface of the magnesium target. The liquid depth above the target surface was several millimeters. An acousto-optically Q-switched Nd-YAG laser (λ = 1064 nm) with 240 ns pulse duration, was used and adjusted to operate at 210 Hz repetition rate. The laser pulse energy applied on the target was 3.5 mJ, leading to a fluence of about 91 J cm^{-2}. The thickness of the target was 1 mm. The irradiation time in the experiments was 45 min. During the ablation in acetone, the spark plumes become larger with a cracking noise. Small bubbles were observed and suggest that acetone was pyrolized during the laser ablation process. Upon irradiation of a laser beam, the color of the solution turned light metallic gray. Structures were not stable and the rapid agglomeration even pending the laser ablation process. These agglomerations precipitated at the bottom of the container, rapidly.

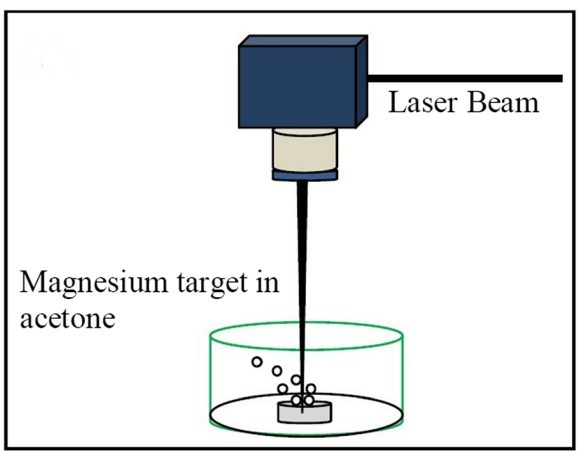

Fig. 1 Laser ablation of magnesium target in acetone and formation of Mg/MgO microstructures

Structural characterization

After laser ablation, a small amount of colloidal solution was transferred into a quartz cell for UV–VIS spectroscopy analysis. The optical absorbance of the sample was measured by using a high-resolution spectrophotometer, Camspec, ModelM350 in the wavelength range of 200–1000 nm.

X-ray diffraction patterns of structures were recorded by evaporation of the colloidal solutions onto a glass substrate at room temperature. The crystal structure of sample was analyzed by a Philips diffractometer (STADI MP) with Cu K_α radiation, angle step size of 0.02°, and count time of 1.0 s per step.

An amount of wet precipitate was transferred to a quartz vessel placed in the open air to evaporate the liquid in order to acquire some powder for FTIR investigations. The FTIR spectrum is prepared by a Therno Nicollet NEXUS 870 FT_IR model spectrophotometer.

Some drops of Mg/MgO colloidal solution have also been deposited onto an Aluminum plate in order to perform SEM analysis with a TS5136MM microscope operating at 30 kV.

Z-scan setup

By using the Z-scan setup can be measured the sign and magnitude of the nonlinear refractive index (n_2) and nonlinear absorption coefficient (β), simultaneously. The Z-scan technique has sensitivity analogous to interferometric methods [23].

The experimental setup for Z-scan is shown schematically in Fig. 2. A Q-switched Nd-YAG laser (Ekspla NL640 model, 532 nm, 10 ns, 200 Hz) was used as the light source. The sample was traveled in the direction of the light propagation near the focal spot of the lens. The radius of the beam waist ω_0 was calculated to be 37 μm at the focal point. The Rayleigh length, $z_0 = \pi\omega_0^2/\lambda$ was estimated to be 8.08 mm, much greater than the thickness of the sample, which is an indispensable requisite for Z-scan experiments.

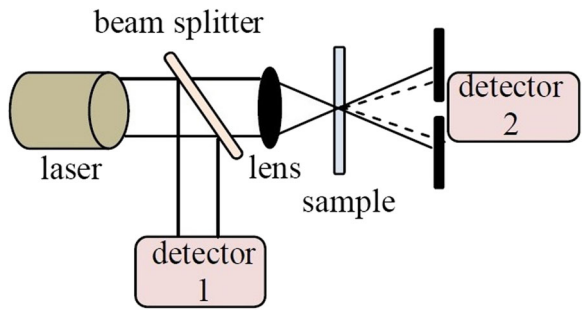

Fig. 2 Schematic diagram of the experimental setup for the measurement of nonlinear optical parameters of Mg/MgO structures prepared in acetone

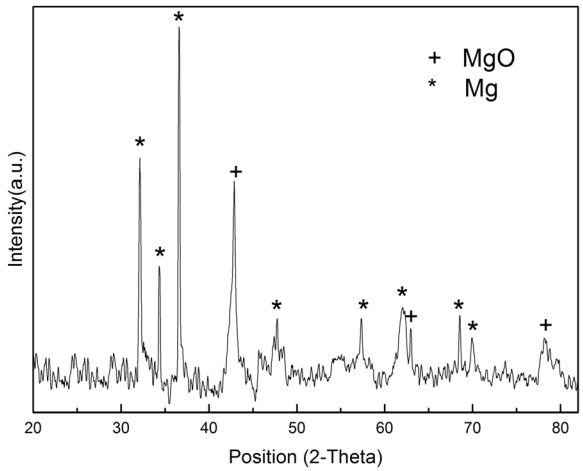

Fig. 3 XRD pattern of Mg/MgO structures prepared by using the laser ablation method

The intensity of the laser beam is 1.1×10^8 Wcm^{-2} at the focal point. This setup had been already applied to investigate NLO properties of $Mg(OH)_2$ nanostructures [24].

Results

Structural investigations

The typical XRD pattern of the structures prepared by the pulsed Nd-YAG laser ablation of magnesium target in acetone is given in Fig. 3. The XRD pattern indicates that both MgO and Mg are presented in the sample with a higher percentage of Mg. It is clear from the XRD pattern that the prepared powders are polycrystalline structures inclusive Mg and MgO. The weight percentage of each Mg and MgO structures can be calculated by Rietveld method [25]. The Mg/MgO ratio in the final product synthesized by laser ablation of magnesium target in acetone is 65/35 percentage. The formed phases in the XRD pattern of Mg/MgO microstructures are the same of those are reported by Phuoc et al. and Abrinaei et al [20, 21].

During the ablation process, each laser pulse with quite high energy passes through the acetone above the magnesium target and increases its temperature. When the front part of the laser pulse interacts with the target, it induces a plasma plume on the surface, which is quite massive. Hence, the heat that is transferred between hot confined plasma and the surrounding liquid increases the temperature of the liquid.

The Mg/MgO microstructures could be formed in three stages. In the first stage, after the interplay among magnesium target and laser beam, the high-temperature and high-pressure plasma is generated in the magnesium target and acetone interface. In the next step, the Mg clusters are produced because of successive ultrasonic and adiabatic expansion of the high-temperature and

high-pressure magnesium plasma that makes a cold zone of magnesium plume [26, 27]. In this experiment, the interval between two consecutive pulses of Nd-YAG laser is 0.005 s (repetition rate is 200 Hz) and it is much longer than the lifetime of the magnesium plasma plume. Hence, the next laser pulse does not interact with the previous plasma plume. In the third step, the plasma quenches and the produced Mg clusters envisage the acetone and occur some chemical reactions and lead to the formation of Mg/MgO microstructures. Outwardly, Mg clusters generated by laser ablation of Mg in acetone were oxidized in this solvent, possibly under the high-energy conditions via reaction with the oxygenated solvent. The observed color changes in acetone suggested that the solvent was altered or decomposed due to laser heating or reaction with the Mg particles [28].

Optical properties

Figure 4 shows the UV-VIS optical absorption spectrum of the colloidal suspension of the sample in acetone. Obviously, there is a characteristic absorption band at about 410 nm.

The measurement of the energy band gap, E_g, is important in the micro- and nano-materials. There are various methods for calculation of E_g. In this work, the energy band gap was determined using UV-Vis absorption spectrum of Mg/MgO microstructures. The derivative method was applied for measurement of E_g. In this method, the first derivative of the absorbance was evaluated near the fundamental absorption edge, leading to E_g [29]. The energy band gap value is obtained equal to 2.3 eV for Mg/MgO microstructures.

The electron configuration of magnesium is $1\ s^2\ 2\ s^2\ 2p^6\ 3\ s^2$ that 3 s shell is full. Then, the 3 s shell of Mg would not allow for electrons to increase energy on its own if the 3p band was separated by a gap from the 3 s band. But, in magnesium the energies of 3 s and 3p bands overlap and the 3p band can incorporate six electrons per atom (2 (2 l + 1) =6), overall 3 s and 3p orbitals from a band can incorporate eight electrons. Consequently, the quarter of conduction band in magnesium is full merely. Thus, magnesium is a good conductor while magnesium oxide is close to an ideal insulating ionic solid with a valence band structure dominated by the strong potential of the ionic cores [19].

The calculated band gap of Mg/MgO microstructures synthesized by the laser ablation method in acetone is significantly smaller than the wide band gap energy 7.8 eV expected for the bulk, pure, crystalline MgO. Therefore, it is clear that Mg/MgO microstructures have metallic conduction behavior [18].

FTIR transmittance spectrum in the wave number range of 4000–500 cm^{-1} for the Mg/MgO microstructures produced by laser ablation of Mg in acetone is presented in Fig. 5.

In the FTIR spectrum, the stretching bands of the superficial OH groups are seen in the region between 4000 and 3500 cm^{-1}. The absorption band around 3448 cm^{-1} is broad and corresponds to the –OH-group-stretching vibration that is dedicated to –OH-stretching mode of residue water and absorbed acetone on the surface of Mg/MgO microstructures. This peak shows the presence of hydroxyl groups at low coordination sites or defects [30]. The absorption bands around 2926 and 2851 cm^{-1} are due to surface OH stretch appearing from hydroxyl groups in dissociated state or C–H stretch of organic residue [31], where these peaks are due to surface OH stretch in-phase and out of phase, respectively. The peak at 1672 cm^{-1} was attributed to the bending

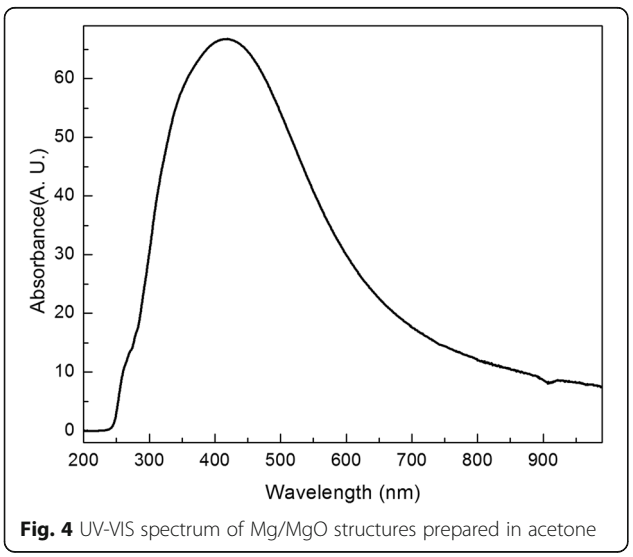

Fig. 4 UV-VIS spectrum of Mg/MgO structures prepared in acetone

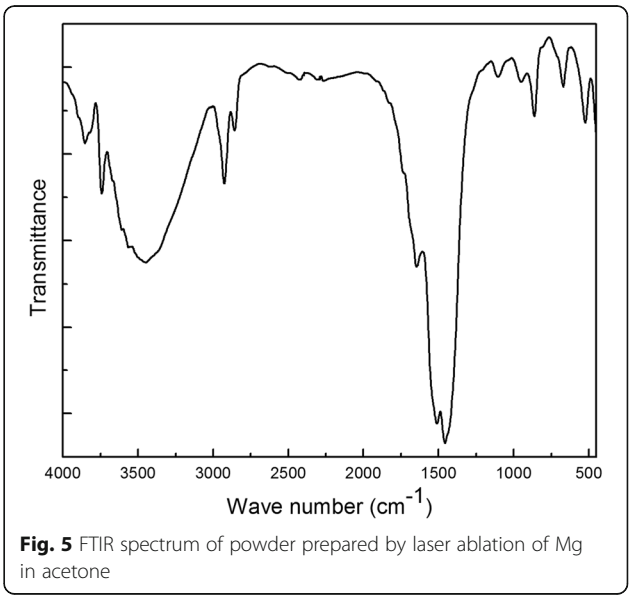

Fig. 5 FTIR spectrum of powder prepared by laser ablation of Mg in acetone

vibration of the water molecule. An absorption peak at 1457 cm^{-1} is assigned to ν_a (C–O) + δ (OC = O) modes. Thus, these contain signatures of adsorption and chemisorption of water and acetone. Tow sharp absorption peaks at 1107 and 970 cm^{-1} are devoted to C–O/C–O stretching modes. While the band at 861 cm^{-1} corresponds to ν (Mg–O) + δ (O–C = O), a peak at 673 cm^{-1} is ascribed to bending mode of O = C = O or vibration of water. The two peaks at 450 cm^{-1} and 515 cm^{-1} affirmed the presence of Mg-O vibrations [32].

Morphological properties

The morphology of the structures examined by scanning electron microscopy (SEM) is shown in Fig. 6.

The SEM image shows that the Mg/MgO microstructures are constructed of particles in the nearly square shape. The obvious SEM picture of Mg/MgO structures was obtained after about 10,000 times grandiosity. The lines appeared in this image related to aluminum foil on which colloidal solution was dried.

The corresponding particle size distribution of the mean sizes is shown in Fig. 7. As shown in the figure, the size distribution width becomes narrow from 1 to 1.5 μm.

Phuoc et al. prepared Mg/MgO nanoparticles in acetone and isopropanol by Nd: YAG (λ = 1064 nm) laser ablation of a magnesium target with distribution sizes were ranged from 15 to 20 nm up to 50 – 100 nm [20]. Abrinaei et al. applied the Nd-YAG (λ = 1064 nm) and cooper vapor laser beam and formed the Mg/MgO spherical and plate-like nanostructures and cubic microstructures with distribution sizes were ranged from 80 to 100 nm and 1–1.1 μm, respectively [21]. As a comparing the results, it approved the results of previous work's author that showed the parameters of laser and liquid medium in laser ablation experiment significantly alter the shape and size of resultant products [21].

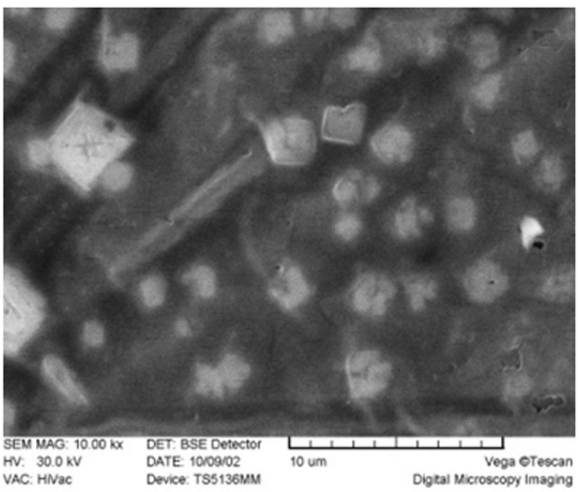

Fig. 6 SEM image of Mg/MgO microstructures generated by using laser ablation of magnesium target in acetone

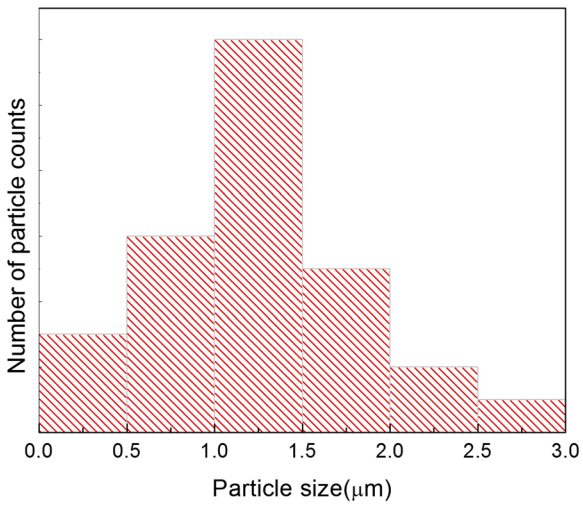

Fig. 7 Particle size distribution of structures generated in acetone

Nonlinear optical properties

NLO parameters, the nonlinear refractive index (n_2) and nonlinear absorption coefficient (β) of the colloidal Mg/MgO structures were obtained by the following relationships [23]:

$$T_{norm} = Ln(1 + q_0(z,t))/q_0(z,t) \quad (1)$$

$$q_0(z,t) = \beta I L_{eff}/\left(1 + z^2/z_0^2\right) \quad (2)$$

$$L_{eff} = \left(1-e^{-\alpha L}\right)/\alpha \quad (3)$$

$$\alpha = -(1/L)Ln(I/I_0) \quad (4)$$

$$\left|\Delta T_{p-v}\right| = 0.406(1-S)^{0.25}(2\pi/\lambda)n_2 I L_{eff} \quad (5)$$

Where T_{norm} is the normalized transmission in the open-aperture Z-scan setup and $q_0(z,t)$ is a dimensionless factor, ΔT_{p-v} is the normalized difference between the peak and the valley in the curve of normalized transmittance (T_{norm}) versus location of the sample (z). In these equations, λ is the wavelength of radiation (532 nm), I is the intensity of radiation, S is the fraction of radiation detected by the detector (the transmittance of the aperture), α is the linear absorption coefficient, L refers to the sample length (1 mm), and L_{eff} is an effective sample thickness, which was measured by OL setup shown in Fig. 2.

Optical limiting

In the recent years, the selection of NLO materials in which increase influence of light leads to significant decreases in transmittance is taken into consideration.

These materials are used for optical power limiters devices. Investigating of new materials as the optical limiter is important for the protection of a person's eye and optical sensors from laser irradiation. In this work, the OL experiment was carried out by locating the sample at focus location and evaluating the transmitted power thru the aperture for several incident laser powers. By the OL consideration, the critical power of the laser beam at which the nonlinearity starts to affect the transmission can be measured. It is evident that the materials are suitable for OL applications that possess the lower OL threshold.

The experimental setup for OL measurements is shown in Fig. 2. In the OL configuration, the aperture is not used. The sample is put near the focal plane of the lens and the input power is changed after crossing the sample. A 50% beam splitter divides the initial power into the half. The power meter 1 is used to measure the input power. The output power of the transmitted beam through the Mg/MgO solution is measured by power meter 2.

The plot of output power versus input power for Mg/MgO microstructures synthesized by laser ablation of magnesium target in acetone is shown in Fig. 8. A threshold is attained at 20 mW of the input power. After 20 mW, the output power stabilized against the input power. At a low incident power up to 20 mW, the output power alters linearly with a ratio of $I/I_0 = 0.89$. By using the Eq. (4), the linear absorption coefficient for these microstructures is obtained: $\alpha = 1.16\ cm^{-1}$.

The plot of output power versus input power for Mg/MgO nanostructures synthesized by laser ablation of magnesium target in isopropanol is shown in Fig. 9. A threshold is reached at 20 mW of the input intensity with slight variation in the output intensity for larger amounts of the input intensities. At a low incident power up to 20 mW, the output power alters linearly with a ratio of $I/I_0 = 0.88$. By using the Eq. (4), the linear absorption coefficient for nanostructures prepared by laser ablation of magnesium target in isopropanol is obtained: $\alpha = 1.27\ cm^{-1}$.

The OL results confirm that structures prepared by laser ablation of Mg target in acetone and isopropanol are good candidates for OL at 532 nm pulsed lasers.

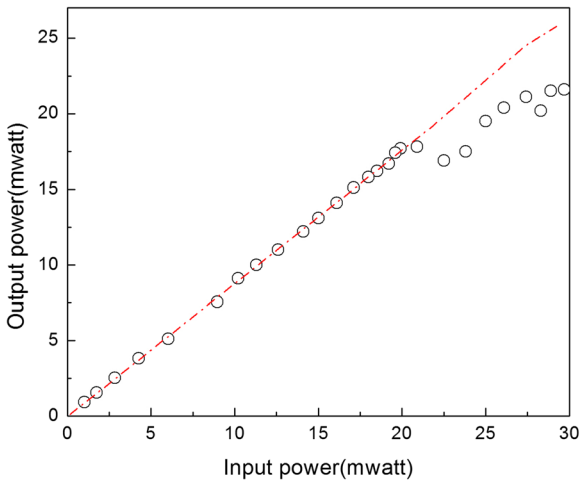

Fig. 9 The plot of output power versus input power for Mg/MgO nanostructures prepared by the laser ablation of magnesium target in isopropanol

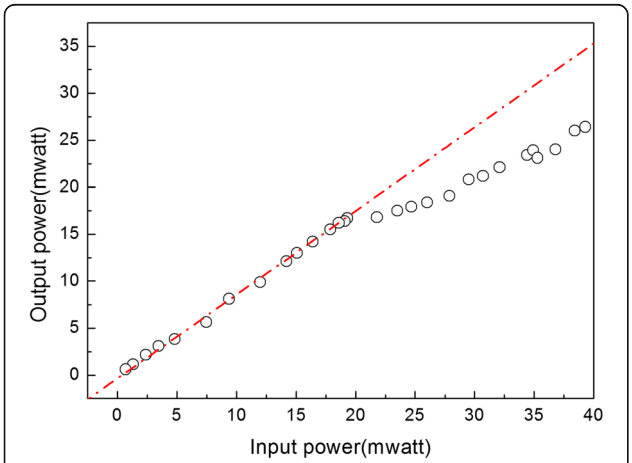

Fig. 8 The plot of output power versus input power for Mg/MgO structures prepared by the laser ablation method in acetone

Closed- aperture Z-scan

The closed-aperture normalized transmittance curve for microstructures synthesized in acetone is shown in Fig. 10. For a sample that exhibits both nonlinear absorption and refraction, their contribution to the far-field beam profile and Z-scan transmittance is coupled. However, it is

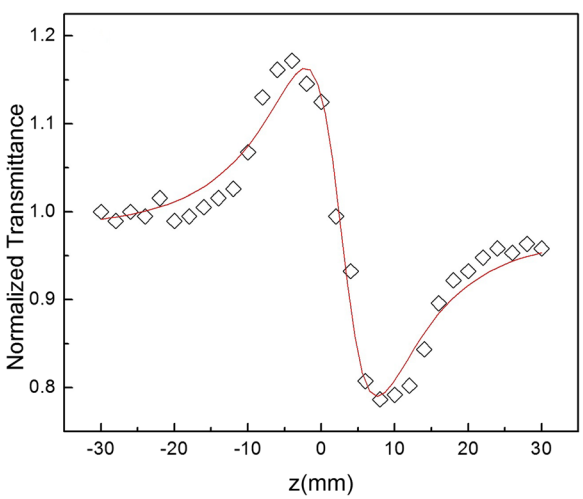

Fig. 10 Closed-aperture Z-scan curve of colloidal Mg/MgO microstructures synthesized in acetone

simple to eliminate the nonlinear absorption contribution to the closed-aperture data. To determine the correct value, the normalized closed-aperture Z-scan data should be divided by the open-aperture Z-scan data to retrieve n_2.

Self-focusing and self-defocusing of laser radiation in nonlinear media is a well-known effect that occurs due to the nonlinear index of refraction n_2. Self-focusing is the effect of positive n_2 while self-defocusing occurs when n_2 is negative. As shown in the Fig. 10, the curves exhibited a peak-to-valley shape indicating a negative value of the nonlinear refractive index, n_2, that shows Mg/MgO microstructures act as a self-defocusing material.

In Fig. 10, the solid curve shows the theoretical fit to the experimental data. The nonlinear refractive index can be measured by fitting the experimental data with the Eq. (5). The nonlinear refractive index of the synthesized structures in acetone is obtained equal to 8.2×10^{-13} cm^2/W. Here, the value of aperture linear transmission, S, is 0.3.

The closed-aperture normalized transmittance curve for nanostructures formed in isopropanol is shown in Fig. 11. As shown in the Fig. 11, the curves exhibited a peak-to-valley shape indicating a negative value of the nonlinear refractive index, n_2, that shows Mg/MgO nanostructures act as a self-defocusing material.

The solid curve shows the theoretical fit to the experimental data, In Fig. 11. The nonlinear refractive index can be measured by fitting the experimental data with the Eq. (5). The nonlinear refractive index of the synthesized nanostructures in isopropanol media is obtained equal 2.2×10^{-12} cm^2/W.

Open-aperture Z-scan

The open-aperture Z-scan allows measuring the nonlinear absorption coefficient, β. When the sample is located far from the focal point, the laser radiation intensity is low and T(z) is close to 1. The intensity becomes higher as the sample moves closer to the lens focal point. As the result of the positive nonlinear absorption, T(z) becomes smaller and reaches the minimum at the focal point. In the case of negative nonlinear absorption, the reverse picture occurs.

Figure 12 illustrates the open-aperture Z-scan curve of colloidal Mg/MgO microstructures measured by Z-scan setup. It is seen that the open-aperture transmittance has a minimum transmittance. The minimum transmittance confirms the presence of reverse saturation absorption in Mg/MgO microstructures. A fit of the Eq. (1) to the experimental data (solid curve) is depicted in Fig. 12, and yields the value of the nonlinear absorption coefficient $\beta = 1.15 \times 10^{-8}$ cm/W. The open-aperture z-scan data

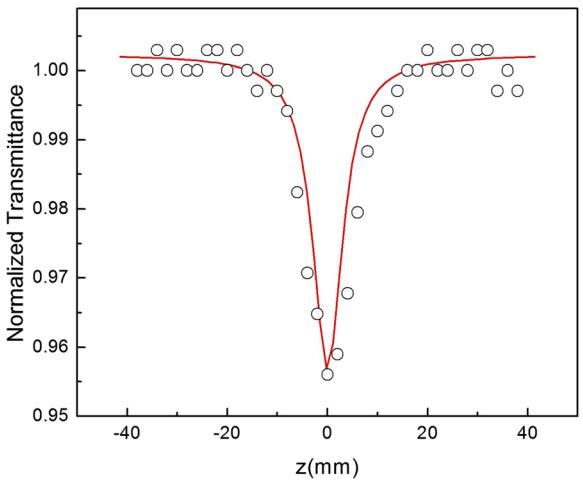

Fig. 12 Open-aperture Z-scan experimental data and theoretical fitting curve for Mg/MgO microstructures prepared in acetone environment

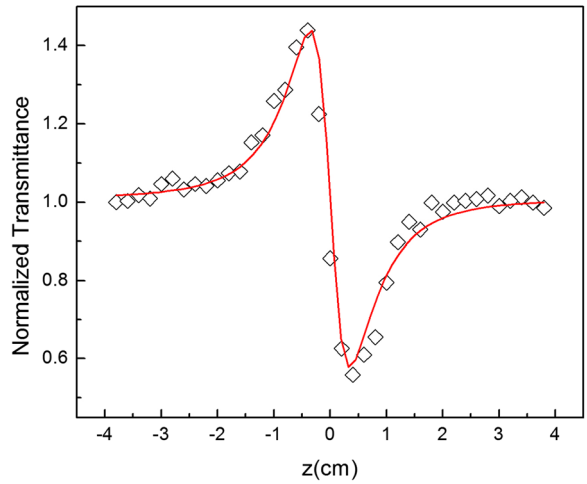

Fig. 11 Closed-aperture Z-scan curve of colloidal Mg/MgO nanostructures prepared in isopropanol

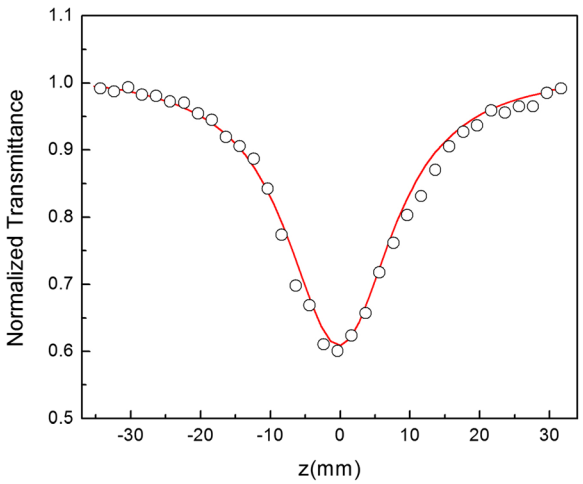

Fig. 13 Open-aperture Z-scan experimental data and theoretical fitting curve for Mg/MgO nanostructures synthesized in isopropanol

for Mg/MgO microstructures synthesized in acetone was fitted with two-photon absorption (2PA) theoretical curve.

The open-aperture normalized transmittance curve for nanostructures formed in isopropanol is shown in Fig. 13. As shown in the Fig. 13, the open-aperture transmittance has a minimum transmittance. The minimum transmittance confirms the presence of reverse saturation absorption in Mg/MgO nanostructures. A fit of the Eq. (1) to the experimental data (solid curve) is depicted in Fig. 13, and yields the value of nonlinear absorption coefficient $\beta = 1.03 \times 10^{-7}$ cm/W. The open-aperture z-scan data for Mg/MgO nanostructures synthesized in isopropanol was fitted to 2PA theoretical curve, properly.

Discussion

The products of ablation simultaneously depend on the properties of the input laser pulses and the surrounding liquid environment [33]. The polarity and the linear refractive index and viscosity of the liquid media, as well as the thickness of the liquid layer on the target surface, are very important in laser ablation process. On the other hands, the parameters of laser that can be effective in products of laser ablation include beam waist, fluence, wavelength, repetition rate, the number of pulses incident per unit area, and pulse duration. Therefore, a minor change in one of these parameters can have a critical impact on products of ablation. The variations of size of products in two cases mentioned in this research are functions of both laser parameters and liquid media.

The calculated values from Z-scan experiments for Mg/MgO microstructures, Mg/MgO nanostructures and $Mg(OH)_2$ structures are shown in Table 1. Furthermore, the real and imaginary parts of $\chi^{(3)}$ are listed in Table 1. The imaginary part of $\chi^{(3)}$ is related to β as [23]:

$$\mathrm{Im}\chi^3(esu) = \left(10^{-2}\varepsilon_0 c^2 n_0^2 \lambda/4\pi^2\right)\beta(cm/W) \quad (6)$$

The real part of $\chi^{(3)}$ is related to n_2 as [23]:

$$\mathrm{Re}\chi^3(esu) = \left(10^{-4}\varepsilon_0 c^2 n_0^2/\pi\right)n_2\left(cm^2/W\right) \quad (7)$$

Table 1 Nonlinear optical parameters of the structures prepared by laser ablation of Mg in acetone, isopropanol and water

Nonlinear optical parameters	Mg/MgO microstructures	Mg/MgO nanostructures	$Mg(OH)_2$ structures [24]
n_2 (cm^2/W)	-8.2×10^{-13}	-2.2×10^{-12}	$+7.76 \times 10^{-13}$
β (cm/W)	1.15×10^{-8}	1.03×10^{-7}	1.01×10^{-7}
Im $\chi^{(3)}$ (esu)	2.75×10^{-6}	2.74×10^{-5}	4.58×10^{-5}
Re $\chi^{(3)}$ (esu)	2.47×10^{-11}	7.43×10^{-11}	4.42×10^{-11}
$\lvert\chi^{(3)}\rvert$ (esu)	2.75×10^{-6}	2.74×10^{-5}	4.58×10^{-5}

Where in Eq. (6) and Eq. (7), n_0 is refractive index, ε_0 is the vacuum permittivity and c is the light velocity in vacuum.

From the Table 1 data, comparing the values of nonlinear refractive indices (n_2) for two samples synthesized in two different liquid environments indicates that n_2 of Mg/MgO microstructures prepared in acetone is an order of magnitude smaller than the value for the n_2 of Mg/MgO nanostructures prepared in isopropanol.

As can be seen in Table 1, comparing the values of the nonlinear absorption coefficient (β) for two samples synthesized by laser ablation of magnesium target in acetone and isopropanol indicates that β for Mg/MgO microstructures is an order of magnitude smaller than the value for the β of Mg/MgO nanostructures. These results show that the Mg/MgO nanostructures are stronger asdsorbent than the Mg/MgO microstructures. Then, the Mg/MgO nanostructures are more appropriate for the protection of eyes and sensors from harmful radiations than the Mg/MgO microstructures.

Therefore, it is clear that a contributing factor in the value of NLO parameters is the particle size of the material.

Furthermore, comparing the results of this study with those of the laser ablation of magnesium in water [24] shows outstanding points. The results of the latter one in the previous study led to the formation of $Mg(OH)_2$ nanostructures and investigation of their NLO properties. The sign of the nonlinearity for $Mg(OH)_2$ nanostructures is opposite to that of Mg/MgO structures.

The low cost of these magnesium-based materials is another advantage that is worth mentioning comparing to other NLO materials. Therefore, each of $Mg(OH)_2$ nanostructure, Mg/MgO microstructure and Mg/MgO nanostructure have its own capability to be used in NLO devices.

A review of the investigation of NLO parameters of semiconductors, fullerenes, dyes, metals, and crystals in various spectral regions was previously reported [34]. Compared to reported amounts in Ref. [34], the Mg/MgO nanostructures and microstructures have satisfactory values despite their low cost.

Conclusion

The major purpose of the present paper is to open a new way to the further development to find suitable materials for producing the highly efficient nonlinear devices that can be used in optical switching and OL.

The pulse laser ablation of magnesium target in acetone led to nearly square Mg/MgO microstructures in the range of 1–1.5 μm with a narrow size distribution. These structures possessed dramatic linear and NLO properties. XRD pattern confirmed the formation of Mg/MgO microstructures. UV-VIS spectrum indicated a

characteristic absorption band at about 410 nm. The energy band gap of Mg/MgO microstructures calculated equal to 2.3 eV.

Laser ablation of a magnesium target in acetone and isopropanol is shown to be a convenient approach by which to fabricate magnesium-based optical limiters devices.

The nonlinear refraction index, n_2, for Mg/MgO microstructures and nanostructures is negative and of the order of 10^{-13} cm^2/W and 10^{-12} cm^2/W, respectively. The negative sign of n_2 indicates that the self-defocusing phenomenon has taken place and these structures can be considered as a thin negative lens. A nonlinear absorption was detected and is mainly associated with the reverse saturation absorption. The nonlinear absorption coefficient (β) was of the order of 10^{-8} cm/W and 10^{-7} cm/W for Mg/MgO structures synthesized in acetone and isopropanol, respectively.

The third-order optical nonlinearities, $\chi^{(3)}$, are calculated using $|\chi^3| = [(Re(\chi^3))^2 + (Im(\chi^3))^2]^{1/2}$ equation for Mg/MgO microstructures and nanostructures 2.75×10^{-6} and 2.74×10^{-5} esu, respectively.

These results show that the size of the Mg/MgO structures is an effective factor in the order of magnitude of NLO parameters. As well, Mg/MgO microstructures and nanostructures synthesized by the Ng-YAG laser ablation of Mg target in acetone and isopropanol are promising materials for applications in NLO devices.

Abbreviations
2PA: Two-photon absorption; FTIR: Fourier transform infrared spectroscopy; NLO: Nonlinear optical; OL: Optical limiting

Acknowledgements
Not applicable.

Funding
Not applicable.

Availability of data and materials
The datasets supporting the conclusions of this article are included within the article.

Competing interests
The author declares that she has no competing interests.

Consent for publication
Not applicable.

Ethics approval and consent to participate
Not applicable.

Publisher's Note

Received: 15 February 2017 Accepted: 20 April 2017
Published online: 01 May 2017

References
1. Boyd, R.W.: Nonlinear optics. Academic, New York (2003)
2. Jeong, H., Mark, A.G., Fischer, P.: Magnesium plasmonics for UV applications and chiral sensing. Chem Commun **52**, 12179–12182 (2016)
3. Sterl, F., Strohfeldt, N., Walter, R., Griessen, R., Tittl, A., Giessen, H.: Magnesium as novel material for active plasmonics in the visible wavelength range. Nano Lett **15**(12), 7949–7955 (2015)
4. Kooi, BJ, Palasantzas, G, Hosson, JThMDe: Gas-phase synthesis of magnesium nanoparticles: A high-resolution transmission electron microscopy study. Appl. Phys. Lett. 89, 161914-1-3 (2006).
5. Zaluska, A., Zaluski, L., Strom-olsen, J.O.S.: Structure, catalysis and atomic reactions on the nano-scale: a systematic approach to metal hydrides for hydrogen storage. Appl Phys A Mater Sci Process **72**(2), 157–165 (2001)
6. Gao, T., Han, F., Zhu, Y., Suo, L., Luo, C., Xu, K., Wang, C.: Hybrid Mg^{2+}/Li^{+} battery with long cycle life and high rate capability. Adv Energy Mater **1401507**, 1–5 (2014)
7. Habibi, M.K., Joshi, S.P., Gupta, M.: Hierarchical magnesium nano-composites for enhanced mechanical response. Acta Mater **58**, 6104–6114 (2010)
8. Locatelli, E., Matteini, P., Sasdelli, F., Pucci, A., Chiariello, M., Molinari, V., Pini, R., Comes Franchini, M.: Surface chemistry and entrapment of magnesium nanoparticles into polymeric micelles: a highly biocompatible tool for photothermal therapy. Chem Commun **50**, 7783–7786 (2014)
9. Hassan, S.F., Gupta, M.: Development of high strength magnesium copper based hybrid composites with enhanced tensile properties. Mater Sci Technol **19**, 253–259 (2003)
10. Zhang, X., Yang, R., Yang, J., Zhao, W., Zheng, J., Tian, W., Li, X.: Synthesis of magnesium nanoparticles with superior hydrogen storage properties by acetylene plasma metal reaction. Int J Hydrogen Energ **36**, 4967–4975 (2011)
11. Al-Gaashani, R., Radiman, S., Al-Douri, Y., Tabet, N., Daud, A.R.: Investigation of the optical properties of $Mg(OH)_2$ and MgO nanostructures obtained by microwave-assisted methods. J Alloy Compd **52**, 71–76 (2012)
12. Ouraipryvan, P., Sreethawong, T., Chavadej, S.: Synthesis crystalline MgO nanoparticle with mesoporous-assembled structure via a surfactant-modified sol-gel process. Mater Lett **63**(21), 1862–1865 (2009)
13. Mirzaei, H., Davoodnia, A.: Microwave assisted sol-gel synthesis of MgO nanoparticles and their catalytic activity in the synthesis of hantzsch 1,4-Dihydropyridines. Chinese J Catal **33**(9), 1502–1507 (2012)
14. Bertinetti, L., Drouet, C., Combes, C., Rey, C., Tampieri, A., Coluccia, S., Martra, G.: Surface characteristics of nanocrystalline apatites: effect of mg surface enrichment on morphology, surface hydration species, and cationic environments. Langmuir **25**, 5647–5654 (2009)
15. Martinez-Boubeta, C., Bacells, L., Cristofol, R., Sanfeliu, C., Rodriguez, E., Weissleder, R., Lope-Piedrafita, S., Simeonidis, K., Angelakeris, M., Sandiumenge, F., Calleja, A., Casas, L., Monty, C., Martinez, B.: Self-assembled multifunctional Fe/MgO nanospheres for magnetic resonance imaging and hyperthermia. Nanomedicine **6**(2), 362–370 (2010)
16. Di, D.R., He, Z.Z., Sun, Z.Q., Liu, J.: A new nano-cryosurgical modality for tumor treatment using biodegradable MgO nanoparticles. Nanomedicine **8**(8), 1233–1241 (2012)
17. Tang, Z.X., Lv, B.F.: MgO nanoparticles as antibacterial agent: preparation and activity. Braz J Chem Eng **31**(3), 591–601 (2014)
18. Kurth, M., Graat, P.C.J., Mittemeijer, E.J.: The oxidation kinetics of magnesium at low temperatures and low oxygen partial pressures. Thin Solid Films **500**, 61–69 (2006)
19. Canney, S.A., Sashin, V.A., Ford, M.J., Kheifets, A.S.: Electronic band structure of magnesium and magnesium oxide: experiment and theory. J. Phys. Condens Matter **11**, 7507–7522 (1999)
20. Phuoc, T.X., Howard, B.H., Martello, D.V., Soong, Y., Chyu, M.K.: Synthesis of $Mg(OH)_2$, MgO, and Mg nanoparticles using laser ablation of magnesium in water and solvents. Opt Laser Eng **46**, 829–834 (2008)
21. Abrinaei, F., Torkamany, M.J., Hantezadeh, M.R., Sabbaghzadeh, J.: Formation of Mg and MgO nanocrystals by laser ablation in liquid: effects of laser sources. Sci Adv Mater **4**, 501–506 (2012)
22. Gutierrez, Y., Ortiz, D., Sanz, J.M., Saiz, J.M., Gonzalez, F., Everitt, H.O., Moreno, F.: How an oxide shell affects the ultraviolet plasmonic behavior of Ga, Mg, and Al nanostructures. Opt Express **24**(18), 20621–20631 (2016)
23. Sheik-bahae, M., Said, A.A., Wei, T.H., Hagan, D.J., Van Stryland, E.W.: Sensitive measurement of optical nonlinearities using a single beam. IEEE J Quantum Elect **26**(4), 760–769 (1990)
24. Abrinaei, F.: Laser ablation of magnesium in water and investigation of optical nonlinearity by Z-scan technique. J Opt Soc Am B **33**(5), 864–870 (2016)
25. Snellings, R., Machiels, L., Mertens, G., Elsen, J.: Rietveld refinement strategy for quantitative phase analysis of partially amorphous zeolitised tuffaceous rocks. Geol Belg **13**, 183–196 (2010)

26. Zhu, S., Lu, Y.F., Hong, M.H.: Laser ablation of solid substrates in a water-confined environment. Appl Phys Lett **79**(9), 1396–1398 (2001)
27. Zeng, H.B., Cai, W.P., Li, Y., Hu, J.L., Liu, P.S.: Composition/structural evolution and optical properties of ZnO/Zn nanoparticles by laser ablation in liquid media. J Phys Chem B **109**(39), 18260–18266 (2005)
28. Foster, M., D'Agostino, M., Passno, D.: Water on MgO (100)—An infrared study at ambient temperatures. Surf Sci **590**(1), 31–41 (2005)
29. Ferreirada Silva, A., Veissid, N., An, C.Y., Pepe, I., Barrosde Oliveira, N., da Silva AV, B.: Optical determination of the direct bandgap energy of lead iodide crystals. Appl Phys Lett **69**, 1930–1932 (1996)
30. Site, L.D., Alavi, A.: Lynden-Bell RM. Structure and spectroscopy of a monolayer of water on MgO (100). J Chem Phys **113**(8), 3344–3350 (2000)
31. Rezaei, M., Khajenoori, M.: Nematollahi B. Synthesis of high surface area nanocrystalline MgO by pluronic P123 triblock copolymer surfactant. Powder Technol **205**, 112–116 (2011)
32. Alavi, M.A., Morsali, A.: Syntheses and characterization of Mg(OH)2 and MgO nanostructures by ultrasonic method. Ultrason Sonochem **17**, 441–446 (2010)
33. Rao, S.V., Podagatlapalli, G.K., Hamad, S.: Ultrafast laser ablation in liquids for nanomaterials and applications. J Nanosci Nanotechnol **14**, 1364–1388 (2014)
34. Ganeev, RA, Usmanov, T: Nonlinear-optical parameters of various media. Quantum Electron + 37 (7), 605-622 (2007).